ISSN 0006-2979, Biochemistry (Moscow), 2017, Vol. 82, No. 4, pp. 490-500. © Pleiades Publishing, Ltd., 2017.
Original Russian Text © O. A. Smitienko, O. V. Nekrasova, A. V. Kudriavtsev, M. A. Yakovleva, I. V. Shelaev, F. E. Gostev, D. A. Dolgikh, I. B. Kolchugina, V. A. Nadtochenko, M. P. Kirpichnikov, T. B. Feldman, M. A. Ostrovsky, 2017, published in Biokhimiya, 2017, Vol. 82, No. 4, pp. 664-676.
Originally published in Biochemistry (Moscow) On-Line Papers in Press, as Manuscript BM16-357, March 13, 2017.

Femtosecond and Picosecond Dynamics of Recombinant Bacteriorhodopsin Primary Reactions Compared to the Native Protein in Trimeric and Monomeric Forms

O. A. Smitienko[1]*, O. V. Nekrasova[2,3], A. V. Kudriavtsev[1,3], M. A. Yakovleva[1], I. V. Shelaev[4], F. E. Gostev[4], D. A. Dolgikh[2,3,5], I. B. Kolchugina[3], V. A. Nadtochenko[4], M. P. Kirpichnikov[2,3], T. B. Feldman[1,3,5], and M. A. Ostrovsky[1,3]

[1]*Emanuel Institute of Biochemical Physics, Russian Academy of Sciences, 119334 Moscow, Russia; E-mail: djolia@gmail.com*
[2]*Shemyakin–Ovchinnikov Institute of Bioorganic Chemistry, Russian Academy of Sciences, 117997 Moscow, Russia*
[3]*Lomonosov Moscow State University, Biological Faculty, 119991 Moscow, Russia*
[4]*Semenov Institute of Chemical Physics, Russian Academy of Sciences, 119991 Moscow, Russia*
[5]*Pirogov Russian National Research Medical University, 1117997 Moscow, Russia*

Received October 22, 2016
Revision received December 20, 2016

Abstract—Photochemical reaction dynamics of the primary events in recombinant bacteriorhodopsin (bR_{rec}) was studied by femtosecond laser absorption spectroscopy with 25-fs time resolution. bR_{rec} was produced in an *Escherichia coli* expression system. Since bR_{rec} was prepared in a DMPC–CHAPS micelle system in the monomeric form, its comparison with trimeric and monomeric forms of the native bacteriorhodopsin (bR_{trim} and bR_{mon}, respectively) was carried out. We found that bR_{rec} intermediate ***I*** (excited state of bR) was formed in the range of 100 fs, as in the case of bR_{trim} and bR_{mon}. Further processes, namely the decay of the excited state ***I*** and the formation of intermediates ***J*** and ***K*** of bR_{rec}, occurred more slowly compared to bR_{trim}, but similarly to bR_{mon}. The lifetime of intermediate ***I***, judging from the signal of ΔA_{ESA}(470-480 nm), was 0.68 ps (78%) and 4.4 ps (22%) for bR_{rec}, 0.52 ps (73%) and 1.7 ps (27%) for bR_{mon}, and 0.45 ps (90%) and 1.75 ps (10%) for bR_{trim}. The formation time of intermediate ***K***, judging from the signal of ΔA_{GSA}(625-635 nm), was 13.5 ps for bR_{rec}, 9.8 ps for bR_{mon}, and 4.3 ps for bR_{trim}. In addition, there was a decrease in the photoreaction efficiency of bR_{rec} and bR_{mon} as seen by a decrease in absorbance in the differential spectrum of the intermediate ***K*** by ~14%. Since photochemical properties of bR_{rec} are similar to those of the monomeric form of the native protein, bR_{rec} and its mutants can be considered as a basis for further studies of the mechanism of bacteriorhodopsin functioning.

DOI: 10.1134/S0006297917040113

Keywords: bacteriorhodopsin, recombinant protein, primary reactions, femtosecond absorption laser spectroscopy

Bacteriorhodopsin (bR) is a membrane protein from *Halobacterium salinarum* that carries out a photoenergetic function – directed proton transport through the cellular membrane. It is a unique object for studying molecular mechanisms of light energy conversion in biological systems [1]. In membranes of halobacteria, bR forms patches called purple membranes in which bR trimers are arranged into a regular hexagonal structure [2]. The stability of this two-dimensional crystal is supported by lipids tightly bound to the protein, such as phosphatidyl glycerophosphate (50%) and sulfo-glycolipids (30%). Acting as a light-dependent proton pump, bR generates electrochemical transmembrane potential used for ATP synthesis [2-5]. bR is a chromoprotein with molecular weight of 26.5 kDa; it consists of apoprotein bacterioopsin and a chromophore group, all-*trans* retinal, bound covalently to K-216 through a protonated Schiff base (SB). bR consists of 248 amino acids tightly arranged in seven transmembrane α helices, some amino acids of which form a chromophore center for retinal insertion.

Absorption of a light quantum causes chromophore isomerization into the 13-*cis* form and is accompanied by several reversible transformations of the bR molecule

Abbreviations: bR, bacteriorhodopsin; bR_{mon}, native bacteriorhodopsin in the monomeric form; bR_{rec}, recombinant bacteriorhodopsin; bR_{trim}, native bacteriorhodopsin in the trimeric form; CD, circular dichroism; DA, dark-adapted; ESA, excited state absorption for the S_1 state of bR; FC, Franck–Condon; GSA, ground state absorption for the S_0 state of bR or its photoreaction products; LA, light-adapted; SB, Schiff base; SE, stimulated emission from the S_1 state of bR.

* To whom correspondence should be addressed.

closed into a photocycle. The photocycle results in proton transport from the inner side of the cell membrane to the exterior medium. During the photocycle, intermediates ***I***, ***J***, ***K***, ***L***, M_I, M_{II}, ***N***, and ***O*** are formed, which differ from the initial bR state in their physicochemical properties and may be differentiated spectrally [6-9]. Changes in the spectral properties of intermediates in the visible light region are determined by conformations of the chromophore and of its immediate protein environment. High levels of bR in native purple membranes, where it is the only protein component, allowed determination of its structure relatively quickly – first, with electron cryomicroscopy, and then with X-ray crystallographic analysis at high spatial resolution [10, 11]. Based on three-dimensional structures of bR and its numerous mutants, molecular mechanisms of light transformation into electrochemical potential of a cell are being studied [12-14]. Despite the large amount of accumulated data, bR studies on the molecular level remain relevant.

An important task in this regard is large-scale accumulation of bR and its mutant forms with altered physicochemical and spectral properties. In this regard, of interest is development of new approaches to obtaining recombinant bacteriorhodopsin, analysis of its properties, and of possibilities for its use and integration into various technical devices. In recent years, systems for expressing mutant bR forms in halobacterial cells have been developed. These systems are based on using deletion variants of halobacteria lacking the bR gene, which may be transformed by specific plasmid vectors containing a certain version of a modified gene [15]. Despite the possibility for obtaining genetically altered bR in the native three-dimensional form, these approaches involve complicated genetic engineering procedures as well as difficulties in cultivating halobacteria. The traditional method of bacteriorhodopsin isolation, developed by Oesterhelt and Stoeckenius in 1974 [16], is a labor- and time-consuming procedure involving ultracentrifugation in a sucrose density gradient with the yield of 20 to 50 mg of purple membranes from 1 liter of halobacterial culture. An alternative to this approach is obtaining bR_{rec} in a bacterial expression system in *E. coli*. We developed one of variant of such a system characterized by a high level of bR_{rec} production in cells, simplicity of cultivation, of isolation procedures for bR_{rec} and renaturation with retinal in lipid–detergent micelles. The final yield of renatured bR_{rec} was ~120 mg from 1 liter of culture [17]. A distinct feature of this expression system is monomeric organization of bR, unlike the native protein that is packed into trimers. The bR_{rec} obtained by us was close to native bR_{mon} in its spectral properties and was characterized by the appearance of a bathochromic shift during light adaptation and its capability for proton transport.

The major spectral differences of the monomeric form of native bR are a shift of the absorption maximum to shorter wavelength from 568 to 552-553 nm for the light-adapted form (LA) and from 560 to 546 nm for the dark-adapted form (DA) [18-20], a decrease in extinction coefficient from 63,000 to 44,000 $M^{-1}\cdot cm^{-1}$ [21, 22], and appearance of a monophasic curve on its circular dichroism (CD) spectrum in the visible range (in contrast to a biphasic curve for trimers) [23]. Additionally, bR_{mon} is less thermally stable than bR_{trim} [24]. The differences in absorption spectra may be analyzed in two aspects: first, during bR_{trim} solubilization, protein–protein and protein–lipid interactions that stabilize bR folding in native membranes are disrupted and, as a result, changes occur in the molecular environment of the retinal binding site. Similar shifts in spectral maxima are observed in the cases of certain mutant bR forms, in which charge redistribution around a retinal molecule occurs [25]. Another reason for a spectral shift may be a change in the ratio of retinal isomers, all-*trans*/13-*cis*, from 90/10-95/5 to 62/38-84/16 for the LA form and from 45/55-50/50 to 40/60 for the DA form of trimer and monomer, respectively [21, 26-30]. On trimer → monomer transition, no qualitative differences in the bR photocycle are observed [31]. However, in bR_{mon} the lifetimes of ***L*** and ***N*** intermediates are significantly shorter and, therefore, ***M*** formation occurs faster by an order of magnitude [8]. These kinetic features reflect the presence of a more flexible monomer conformation allowing the formation of a larger number of various bR conformational states.

The bR_{rec} obtained earlier by expression in *E. coli* in lipid–detergent micelles [32, 33] (as well as bR_{mon}) is characterized by a short-wavelength shift in the maximum of the absorption spectrum to 559 nm for the LA form and to 551 nm for the DA form, a decreased extinction coefficient of 52,000 $M^{-1}\cdot cm^{-1}$, and by its capability for proton transport. The ratio of bR_{rec} retinal isomers (all-*trans*/13-*cis*) – 96/4 (LA form) and 39/61 (DA form) – corresponds approximately to bR_{trim}.

In the last decade, ultrafast dynamics of the retinal excited state was studied by the method of pump–probe femtosecond laser absorption spectroscopy in both the native trimeric form and the monomeric form of bR [18, 34-39]. Currently, bR_{trim} primary reactions occurring in the femtosecond and picosecond time range are most often represented by the following scheme: $bR_{568}(h\nu) \rightarrow$ FC(100-200 fs) → $\boldsymbol{I}_{460}$(500 fs) → $\boldsymbol{J}_{625}$(3-5 ps) → $\boldsymbol{K}_{590}$, where FC is the Franck–Condon state of the bR_{568} molecule. Under the action of a light quantum, the ground state of bR_{trim} transits into the excited FC state, which relaxes into intermediate ***I*** over the course of 100-200 fs with a prominent absorption signal (ΔA_{ESA}) in the range of 450-490 nm and a signal of stimulated emission (ΔA_{SE}) in the range of 800-1200 nm [34, 39]. Intermediate ***I*** transforms into the ground state over the course of 500 fs with formation of intermediate ***J*** (quantum yield of 0.64 [40]), accompanied by the transition of retinal from all-*trans* to the 13-*cis* form [37, 38]. After 3-5 ps, intermediate ***J*** transforms into the next intermediate ***K*** with a more relaxed 13-*cis* retinal [41, 42].

During bR monomerization, primary photocycle events change only slightly. The spectral maxima of the excited state ***I***, as well as intermediates ***J*** and ***K***, are practically identical for bR_{mon} and bR_{trim} [18]. The main difference is in kinetic characteristics of the primary photocycle product formation for a trimer and a monomer, which are expressed as following. The transition of the excited state ***I*** into intermediate ***J*** is 0.45-0.55 ps for bR_{trim} (95-100%) [18, 43, 44]; in the case of a monomer, two components appear with lifetimes (relative amplitudes) of 0.63 ps (87%) and 3.51 ps (13%) [18]. Another characteristic of the primary photocycle events is stimulated emission of bR in the near-infrared range, which can be used to estimate the lifetime of the excited state. In the case of a trimer, the major fluorescent state relaxation time is 0.44 ps, corresponding to the major time of relaxation for intermediate ***I***. In the case of a monomer, two relaxation components appear as well – 0.55 and 3.5 ps. The slow and fast components were attributed by the authors of [18] to differences in kinetics of relaxation of all-*trans* and 13-*cis* retinal isomers inside the protein. Thus, the ratio of amplitudes of fast and slow components, 83/13, corresponds approximately to the ratio of retinal isomers in the LA form of bR.

Therefore, isomerization of all-*trans* retinal in a trimer or a monomer occurs over the course of approximately the same time interval, within 0.5 ps. So, trimer destruction does not cause changes in photoisomerization dynamics of all-*trans* retinal and, therefore, the trimeric structure of bR is not a catalyst of the primary photocycle events.

To confirm the correct organization of the chromophore center and the whole bR_{rec} protein, it was necessary to analyze the dynamics of primary reactions of bR_{rec} photocycle in detail compared to the native protein. For the comparison, not only the trimeric, but also the monomeric form of native bR was used, since bR_{rec} was obtained in a monomeric form.

The aim of this study was to analyze the spectral characteristics and formation dynamics of bR_{rec} intermediates ***I***, ***J***, and ***K*** compared to the native protein in trimeric and monomeric forms by pump–probe femtosecond laser absorption spectroscopy with excitation by 560-nm pulses and time resolution of 25 fs.

MATERIALS AND METHODS

Preparation of bR_{rec} samples. bR_{rec} was obtained in a *E. coli* expression system according to the study of Nekrasova et al. [17]. After renaturation of bR_{rec} with retinal in lipid–detergent micelles (1% DMPC, 1% CHAPS, 0.2% SDS), the protein was concentrated on Ni-Sepharose High Performance column (V = 2 ml) (GE Healthcare, Sigma-Aldrich) and then desalted on a PD-10 column (GE Healthcare) in buffer A (1% DMPC, 1% CHAPS, 50 mM Na-phosphate buffer, 150 mM KCl, pH 6.0). bR_{rec} concentration was 2.1 mg/ml, with purity coefficient of A_{280}/A_{559} = 1.49 and absorbance of A_{559} = 4.2 OD units.

Preparation of native bR_{trim} samples. Halobacteria (*H. salinarum*) were grown from the ET1001 strain in the Central Scientific-Research Institute of Technology "Tekhnomash". Purple membranes were kindly provided by "Tekhnomash". The sample was a suspension of purple membranes in buffer B (25 mM Na-phosphate buffer, pH 7.0). bR_{trim} concentration was 1.6 mg/ml, with purity coefficient of A_{280}/A_{568} = 1.78 and absorbance of A_{568} = 3.7 OD units. Before the experiment, the sample was treated with ultrasound with power of 90 W for 2-3 min.

Preparation of native bR_{mon} samples. The bR was monomerized by solubilizing native purple membranes in the nonionic detergent Triton X-100. With this type of preparation, the native lipid environment of the bR molecule remains partially preserved [45]. A bR_{mon} sample was prepared under dimmed red light at room temperature. Stock solution of Triton X-100 prepared with Na-phosphate buffer (pH 6.05) was added to a suspension of purple membranes containing bR_{trim} to the final concentration of Triton X-100 – 2% and Na-phosphate – 25 mM. The sample was incubated at room temperature for 20 h with continuous stirring. Then the sample was centrifuged on a Beckman Coulter Optima TM XE centrifuge (80,000*g*, 18°C, 60 min). Extraction efficiency was ~85%, bR_{mon} concentration was 2.5 mg/ml, and absorbance was A_{553} = 5.9 OD units. The purity coefficient could not be determined since the detergent strongly absorbs in the UV range.

Stationary absorption spectra for samples were registered with a UV 1700 spectrophotometer (Shimadzu, Japan). Light adaptation was carried out by illumination with a halogen lamp (KGM24-250, 24 V, 250 W) with filters YGL-19 and GL-8 passing the spectral range ~500-600 nm. Dark adaptation was conducted for three days at 4°C or for one day at room temperature.

Circular dichroism. Since formation of the monomeric bR form from the trimeric one is accompanied by a rapid change in the CD spectrum [23], to monitor bR monomerization the following spectra were registered (Fig. 1). Registration was carried out with a SKD-2M device (Institute of Spectroscopy, Russian Academy of Sciences) with a thermostatted cell at room temperature. To increase the signal-to-noise ratio, every spectrum was recorded four times in increments of 2 nm. A distinct shift was observed from the biphasic CD spectrum of bR_{trim} with maxima of the positive band at 535 nm and of the negative band at 595 nm to the monophasic spectrum of bR_{mon} with a non-distinct maximum at 560 nm. This indicated destruction of the bR_{trim} hexagonal lattice and trimeric structure and formation of detergent micelles containing single bR_{mon} molecules.

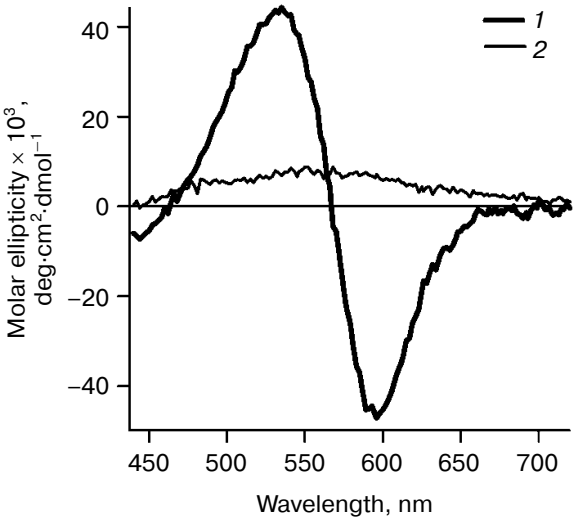

Fig. 1. CD spectra registered for bR_{trim} (*1*) and bR_{mon} (*2*) in the spectral range of 440-720 nm.

HPLC analysis of retinal isomers. Retinal isomers were extracted following the method described in [46]. A 2-ml sample was treated with 1 ml of formaldehyde, mixed, and incubated for 2 min. Then 1.5 ml of methylene chloride was added, and the mixture was intensively shaken and incubated for 10 min. Then 1.5 ml of hexane was added, and the mixture was shaken and centrifuged with a MLW K 26 D centrifuge (680*g*, 10 min). The upper layer containing methylene chloride, hexane, and free retinal isomers was collected and evaporated using the vacuum of a water-jet pump. All procedures were carried out under dim red light.

Chromatographic analysis was carried out on a HPLC system Smartline 1000 (Knauer, Germany) using a K-2500 variable-wavelength spectrophotometric detector. Measurements were taken at the wavelength of 365 nm. The retinal isomers were separated on a Silica column (7 μm, 250 × 4.6 mm; IBM Instruments, USA). Hexane–ethyl acetate solvent mixture (7% v/v) with the addition of absolute methanol (100 μl for 1 liter of the mixture) was used as the eluant at flow rate 1 ml/min.

Femtosecond spectroscopy. Photoinduced absorption spectra were measured with a femtosecond setup using the pump–probe method [44-47]. The sample was excited by Gaussian pulses with recurrence frequency of 60 Hz, duration of 25 fs, wavelength of 560 nm, and energy of 120 nJ. The diameter of the excitation beam in the sample was 300 μm. For the probe pulse, a supercontinuum was generated in a quartz cuvette containing water. The probing pulse energy did not exceed 10 nJ. The diameter of the probing beam was 100 μm. Polarization of the probing pulse in relation to the excitation pulse was rotated by 54.7° ("magic angle"). After the sample, the supercontinuum pulse was directed to an Acton SP-300 polychromator (Princeton Instruments, USA) and detected by a CCB-camera Roper Scientific SPEC-10 (Roper Scientific, Germany). Differential absorption spectra $\Delta A(\lambda)$ were recorded in the spectral range of 400-900 nm.

In spectral ranges of 535-600 and 790-835 nm the ΔA signal could not be registered due to a high level of noise caused by specific features of preparation of the excitation 560 nm pulse. The probing supercontinuum pulse was applied with delay time of 0-3 ps in increments of 3.3 fs, and 3-10 ps in increments of 10 fs with accumulation of signals from 50 spectra. Control differential spectra were also registered with the delay time of 100 ps with accumulation of signals from 5000 spectra to track sample degradation during the experiment. All experiments were carried out at 21°C in a 0.5-mm quartz flow cuvette with window thickness of 0.1 mm. The flow rate allowed the sample to be completely refreshed after each laser pulse. For bR molecules to be in the LA form during excitation by a fs-pulse, the sample circulating in the flow system was constantly illuminated by a continuous laser with wavelength $\lambda = 532$ nm, power $P = 0.02$ mW/cm^2, and diameter $d = 0.8$ cm in the range other than that of the excitation pulse. Photoadaptation of a sample was verified spectrally.

Experimental data were processed with Span software written in the language environment of Matlab.

RESULTS

Spectral properties of bR_{trim}, bR_{mon}, and bR_{rec}. Stationary absorption spectra were registered for samples of bacteriorhodopsin in trimeric and monomeric forms and of the recombinant protein (Fig. 2).

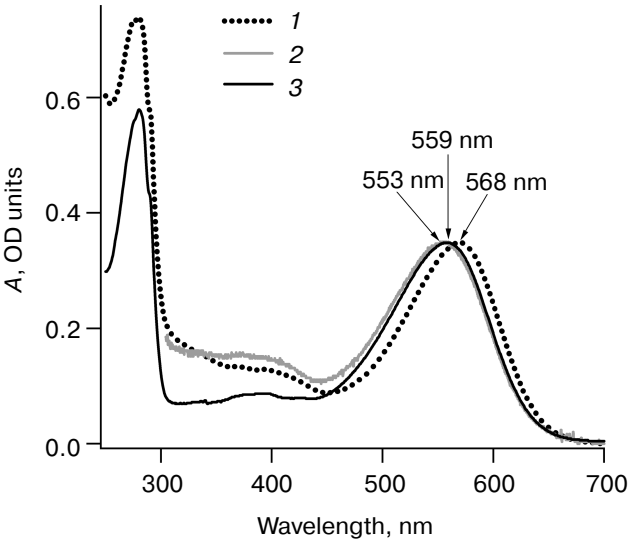

Fig. 2. Stationary absorption spectra for LA samples of bR_{trim} (*1*), bR_{mon} (*2*), and bR_{rec} (*3*). The bR_{mon} spectrum was registered only in the 305-700 nm range since Triton X-100 detergent has intense absorption at wavelength <300 nm. The spectra were normalized by the α-band intensity.

Table 1. All-*trans* and 13-*cis* retinal content in LA and DA samples of bR_{trim}, bR_{mon}, and bR_{rec} and the maxima for stationary absorption spectra of the samples

Sample	Ratio of retinal isomers (%)		λ_{max}, nm
	all-*trans*	13-*cis*	
bR_{trim}(LA)	89	11	568
bR_{trim}(DA)	49	51	560
bR_{mon}(LA)	71	29	553
bR_{mon}(DA)	46	54	547
bR_{rec}(LA)	88	12	559
bR_{rec}(DA)	56	44	552

Figure 2 shows the maxima of sample absorption spectra – 568 nm for bR_{trim}, 553 nm for bR_{mon}, and 559 nm for bR_{rec}, which corresponds to data from the literature [18, 20, 27, 32, 33, 48]. Differences in absorption spectra may be explained by the fact that during bR_{trim} solubilization, protein–protein and protein–lipid interactions are disrupted, which stabilize bR folding in native membranes. This results in changes in the molecular environment of the retinal binding site and in the conformation of retinal itself, increasing the energy of the $S_0 \rightarrow S_1$ phototransition. It should be noted that the bR_{rec} absorption spectrum is more like bR_{mon} in the red range (Fig. 2), which may indicate a similar structure of the chromophore center and chromophore conformation.

HPLC analysis of retinal isomers. To estimate the ratio of all-*trans* and 13-*cis* retinal in the analyzed samples by HPLC, chromatograms were registered for retinals extracted from LA and DA samples of bR_{trim}, bR_{mon}, and bR_{rec} (Fig. 3). The percentage ratio of retinal isomers is provided in Table 1.

As seen in Table 1, the ratio of all-*trans*/13-*cis* retinals (in percent) in the LA sample of bR_{trim} was 89/11, which is slightly less than in other studies [29, 30]. A similar ratio was found for LA samples of bR_{rec} – 88/12, while for bR_{mon} it was 71/29, which is in accordance with published studies [21, 28]. In DA samples of bR the ratio of all-*trans*/13-*cis* retinals decreased to 49/51 for bR_{trim}, 46/54 for bR_{mon}, and 56/44 for bR_{rec}.

Comparison of photoinduced absorption spectra of bR_{trim}, bR_{mon}, and bR_{rec}. Figure 4 shows normalized spectra of photoinduced absorption for three LA samples of bR with delay times of 0.1, 0.6, 1.3, and 9 ps.

Figure 4a shows that within 100 fs after excitation the formation of a pronounced excited state absorption band is observed (ΔA_{ESA}) in the 450-490 nm range for all three samples, which characterizes intermediate ***I*** formation. During the next 1.3 ps this band decreases significantly, and in the 650-nm range the absorption band of the next intermediate ***J*** (ΔA_{GSA}) is formed. In the 530-640 nm range at the time of 100 fs, a bR bleaching band is observed (ΔA_{BL}) (Fig. 4a), which decreases significantly in the picosecond time range due to the formation of intermediate ***J***, which contributes positively to absorption in this range, and to the transition of a part of bR molecules from the excited to the initial state (Fig. 4, b-d). Within early times in the long-wavelength ranges of 700-790 nm and 835-890 nm, a negative band of stimulated emission of state ***I*** (ΔA_{SE}) is observed (Fig. 4, a and b), which disappears in the picosecond time range. By 9 ps after excitation, the differential spectra consist only of the absorption band of intermediate ***K*** $\Delta A_{GSA}(t = 9$ ps) and the bleaching band of bR $\Delta A_{BL}(t = 9$ ps) (Fig. 4d). The $\boldsymbol{J} \rightarrow \boldsymbol{K}$ transition is accompanied by a shift of ΔA_{GSA} signal to shorter wavelength by approximately 20 nm and a slight decrease in absorption intensity.

Comparison of differential spectra of the studied samples shows that formation time, absorption maximum, and the form of intermediate ***I*** absorption band are practically identical for all three samples ($\lambda_{max} = 470$ nm), except the bR_{rec}; the maximum of this band is shifted to longer wavelength by 7 nm (Fig. 4a and Table 2). The maximum intensity for intermediate ***I*** absorption band in

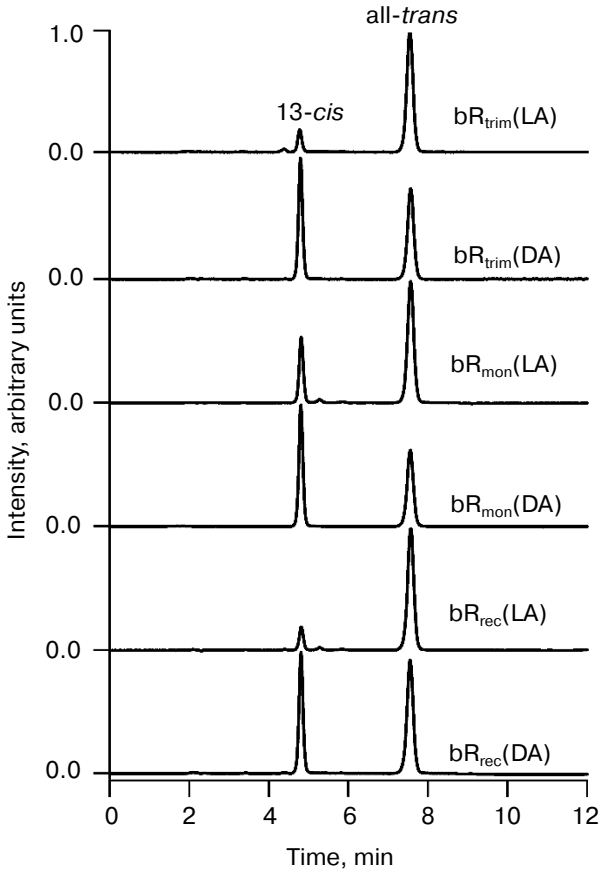

Fig. 3. Normalized chromatograms of retinals extracted from LA and DA samples of bR_{trim}, bR_{mon}, and bR_{rec}. Absorbance was detected at the 365 nm wavelength.

a differential spectrum $\Delta A(\lambda_{max}(\boldsymbol{I}))$ was used to normalize the spectra and kinetic curves represented in Figs. 4 and 5. Within times of 0.6 and 1.3 ps (Fig. 4, b and c), the maximum decrease in absorption is observed for intermediate ***I*** and, therefore, the maximum increase in absorption for intermediate ***J*** of bR_{trim} compared to bR_{mon} and bR_{rec}. This indicates increased time of the $\boldsymbol{I} \rightarrow \boldsymbol{J}$ transition in these samples. As seen in Fig. 4 (c and d), absorption bands of intermediates ***J*** and ***K*** for the bR_{mon} and bR_{rec} samples are shifted to shorter wavelength compared to bR_{trim}. The absorption spectra maxima of intermediate ***K***, registered with delay time of 9 ps, are 625 nm (bR_{mon}), 630 nm (bR_{rec}), and 635 nm (bR_{trim}) (Fig. 4d and Table 2). A shift to shorter wavelength of intermediates ***J*** and ***K*** absorption spectra for bR_{mon} and bR_{rec} samples approximately correlates with the shift in stationary absorption spectra by 15 and 9 nm, respectively (Fig. 2). A similar correlation of absorption spectra maxima for the initial state of bR and the ***K*** form was observed earlier for bR_{mon} [49] and for some bR mutants [42, 50]. It can also be noted that signal ΔA_{GSA} intensity for intermediates ***J*** and ***K*** for bR_{mon} and bR_{rec} samples is decreased by 13-14% compared to that of bR_{trim} (Fig. 4b and Table 2), which may indicate a less effective formation of the ***J*** form and, subsequently, ***K*** form in the photoreaction process.

Comparison of kinetic curves of photoinduced absorption for bR_{trim}, bR_{mon}, and bR_{rec}. Based on the differential spectra (Fig. 4), the time-resolved signals of

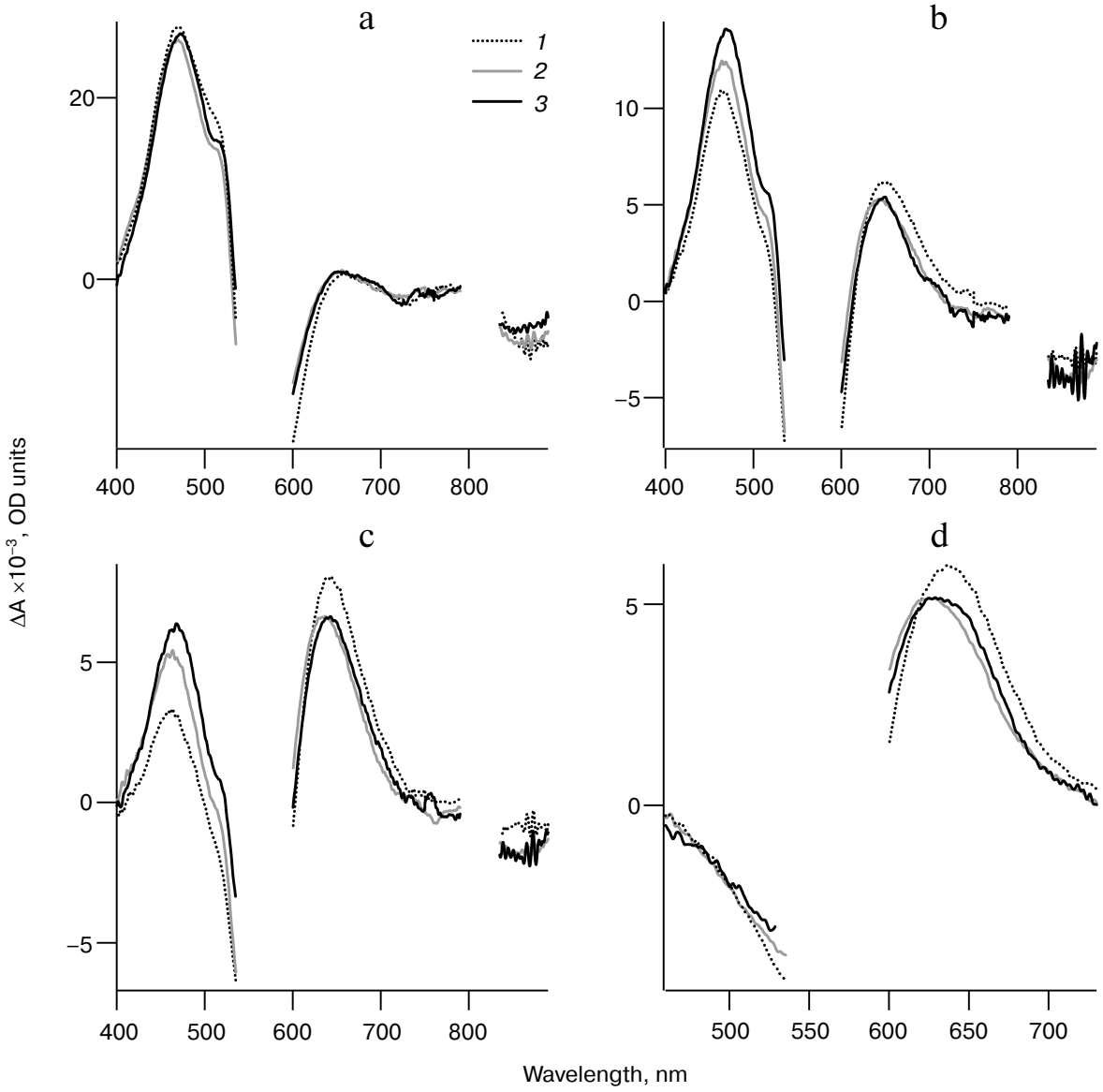

Fig. 4. Normalized spectra of photoinduced absorption for LA samples of bR_{trim} (*1*), bR_{mon} (*2*), and bR_{rec} (*3*) for delay times of 0.1 (a), 0.6 (b), 1.3 (c), and 9 ps (d) in the spectral ranges of 400-890 nm (a-c) and 460-730 nm (d). The curves were normalized to the maximum intensity of the intermediate ***I*** absorption band in the differential spectra.

Table 2. Maxima of absorption bands of intermediates ***I*** and ***K*** in differential spectra of bR_{trim}, bR_{mon}, and bR_{rec} samples registered with delay times of 0.1 and 9 ps, respectively. Relative intensities of the ***K*** intermediate absorption band in differential spectra $\Delta A_{GSA}(\lambda_{max}(\boldsymbol{K}))$ of bR_{trim}, bR_{mon}, and bR_{rec} samples, given in % from $\Delta A_{GSA}(\lambda_{max}(\boldsymbol{K}))$ of bR_{trim} with the delay time of 9 ps

Sample	$\lambda_{max}(\boldsymbol{I})$, nm	$\lambda_{max}(\boldsymbol{K})$, nm	$\Delta A_{GSA}(\lambda_{max}(\boldsymbol{K}), 9\text{ ps})$, %
bR_{trim}	470	635	100
bR_{mon}	470	625	87
bR_{rec}	477	630	86

photoinduced absorption were compared for different LA samples of bR at characteristic wavelengths (Fig. 5, curves *1-3*). For comparison of formation and decay dynamics of intermediate ***I***, kinetic curves were analyzed at wavelengths corresponding to absorption maxima for this intermediate in the differential spectrum (ΔA_{ESA}) (Fig. 5a and Table 2), as well as in a stimulated emission band of bR (ΔA_{SE}) (Fig. 5c). For comparison of intermediates ***J*** and ***K*** formation dynamics for the different bR samples, kinetic curves were analyzed at wavelengths corresponding to absorption maxima of ***K*** in the differential spectrum with a delay time of 9 ps (Fig. 5b and Table 2). Characteristic times of the analyzed processes were estimated by plotting model biexponential curves (Table 3).

As seen from the dynamics of the ΔA_{ESA} signal (Fig. 5a), the appearance of intermediate ***I*** absorption band occurs within 100 fs after excitation for bR_{trim}, 70 fs for bR_{mon}, and 90 fs for bR_{rec}. The decrease in ΔA_{ESA} signal occurs faster for bR_{trim} than for bR_{mon} and bR_{rec}, as was already observed in spectral dynamics of photoinduced absorption for bR samples (Fig. 4, a-c). This process in bR_{trim} is characterized by a fast time component of 0.45 ps (90%) and a slow component of 1.75 ps (10%). In other samples, the fast component increases slightly to 0.52 ps (bR_{mon}) and 0.68 ps (bR_{rec}), and its contribution decreases to ~75%. The slow component for bR_{mon} (1.7 ps) is practically unchanged compared to bR_{trim} (1.75 ps), while for bR_{rec} it is significantly increased (4.4 ps) (Table 3).

In the stimulated emission range of bR at 850 nm, the negative signal ΔA_{SE} for all samples reaches approximately the same intensity by 100-150 fs, after which it begins to decrease in the picosecond time range (Fig. 5c). As well as the ΔA_{ESA} signal, the ΔA_{SE} signal decreases more slowly in bR_{mon} and bR_{rec} compared to bR_{trim}. The fast component of this process is practically the same for all samples being 0.39-0.4 ps, but the contribution of this component decreases sharply for bR_{mon} (46%) and bR_{rec} (54%) compared to bR_{trim} (86%). The slow component is 1.5 ps for bR_{trim}, 1.2 ps for bR_{mon}, and 1.6 ps for bR_{rec} (Table 3).

In the absorption range of intermediates ***J*** and ***K***, the kinetic curves demonstrate the appearance of a negative signal at early times <50 fs, most likely related to both ΔA_{BL} and ΔA_{SE} (Fig. 5b), which shifts to a positive ΔA_{GSA} signal with two characteristic time constants. The first, fast component of signal increase could not be determined due to a significant contribution from an artifact signal at times <90 fs, but it may be approximated as 50-100 fs for all three samples. The following slower rise of the ΔA_{GSA} signal in this spectral range reflects, at times up to 1-2 ps, the dynamics of intermediate ***J*** formation. For bR_{trim}, the characteristic time of this process was 0.4 ps, and the ΔA_{GSA} signal reached its maximum by 1.3 ps (Fig. 5b and Table 3). For the bR_{mon} and bR_{rec} samples, the characteristic time of this process was slightly more, 0.48-0.49 ps, and the ΔA_{GSA} signal reached its maximum by 1.8 ps. Further, in the picosecond time range, a slight

Table 3. Parameters (characteristic times and their contributions) of kinetic curves of photoinduced absorption for bR_{trim}, bR_{mon}, and bR_{rec} obtained by plotting model biexponential curves in time ranges of 0.1-9 ps (470-477 nm) and 0.15-9 ps (625-850 nm) at characteristic probing wavelengths

Sample	λ, nm	t_1, ps	A_1, %	t_2, ps	A_2, %
bR_{trim}	470	0.45 ± 0.007	90	1.75 ± 0.09	10
bR_{mon}	470	0.52 ± 0.001	73	1.70 ± 0.07	27
bR_{rec}	477	0.68 ± 0.005	78	4.40 ± 0.27	22
bR_{trim}	635	0.40 ± 0.01		4.30 ± 0.14	
bR_{mon}	625	0.49 ± 0.01		9.80 ± 1.10	
bR_{rec}	630	0.48 ± 0.01		13.50 ± 2.70	
bR_{trim}	850	0.40 ± 0.01	86	1.50 ± 0.15	14
bR_{mon}	850	0.39 ± 0.03	46	1.20 ± 0.04	54
bR_{rec}	850	0.39 ± 0.03	54	1.60 ± 0.06	46

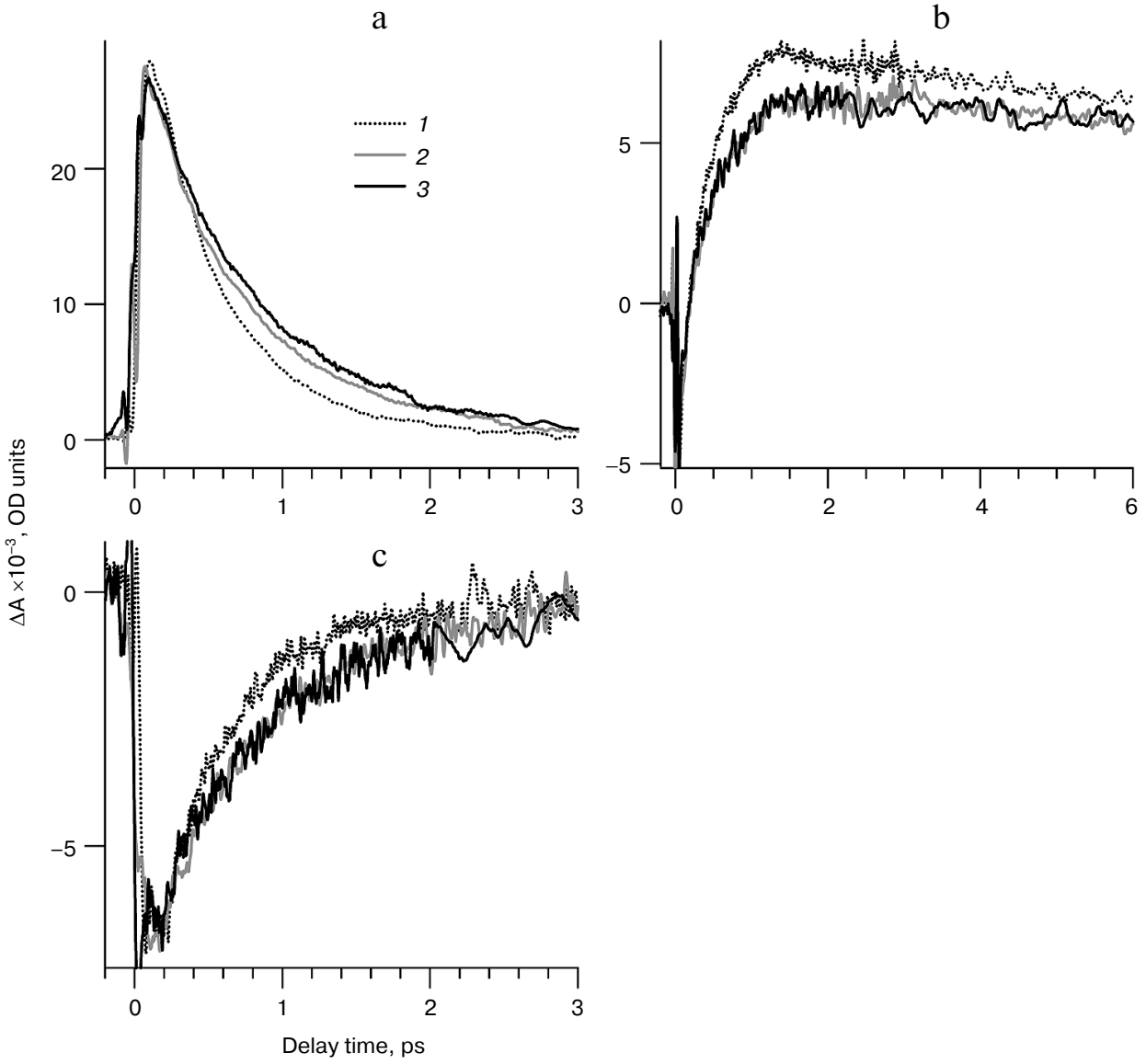

Fig. 5. Normalized kinetic curves of photoinduced absorption for LA samples of bR_{trim} (*1*), bR_{mon} (*2*), and bR_{rec} (*3*), registered at the following probing wavelengths: a) 470 nm (*1*, *2*) and 477 nm (*3*); b) 625 nm (*2*), 630 nm (*3*) and 635 nm (*1*); c) 850 nm. Normalization was to the maximum intensity of intermediate ***I*** absorption band in the differential spectrum.

decrease in absorption is observed, reflecting the process of ***K*** form formation with the absorption maximum shifted to shorter wavelength. The characteristic time of this process for bR_{trim} was 4.3 ps, while for bR_{mon} and bR_{rec} samples, this time increased to 9.8 and 13.5 ps, respectively. Unfortunately, the times of 9.8 and 13.5 ps were determined with low precision, since the kinetic curves were obtained only for times up to 9 ps. The kinetic curves presented in Fig. 5b, as well as differential spectra (Fig. 4d), demonstrated, with times up to 9 ps, reduced ΔA_{GSA} signal by 13-14% for bR_{mon} and bR_{rec} compared to bR_{trim}. As stated earlier, this is most likely caused by a slightly decreased quantum yield of the photoreaction for these samples.

DISCUSSION

In this study, we obtained differential spectra and kinetic curves of photoinduced absorption for bR_{trim}, bR_{mon}, and bR_{rec} samples over a wide spectral probe range, 400-900 nm, within times up to 9 ps. The data obtained for bR_{trim} and bR_{mon} correlate with data from the literature [18, 35, 36, 39]. bR_{rec} demonstrates primary reaction dynamics with characteristics close to those of bR_{mon}, but slightly differing from bR_{trim}. They are: (i) an increase in the excited state lifetime evident in the ΔA_{ESA} band: for the fast component (from 0.45 ps for bR_{trim} to 0.68 ps) and the slow component (from 1.75 ps for bR_{trim} to 4.4 ps) with a decrease in contribution from the fast

component (from 90% for bR_{trim} to 78%) (Fig. 5a and Table 3); (ii) an increase in formation time for intermediates ***J*** (from 0.4 ps for bR_{trim} to 0.48 ps) and ***K*** (from 4.3 ps for bR_{trim} to 13.5 ps) (Fig. 5b and Table 3); (iii) a minor decrease in efficiency of *trans-cis* retinal isomerization reaction in bR_{rec}, judging by a decrease in intensity of intermediate ***K*** absorption band in the differential spectrum by 14% (Figs. 4d and 5b and Table 2). The observed changes in primary reaction dynamics for bR_{rec} and bR_{mon} compared to the native form of bR_{trim} contained in purple membranes and forming a dimeric hexagonal structure are probably connected to the monomeric protein form.

The protein environment is known to strongly control the reaction of retinal isomerization in bR, ensuring its speed, efficiency, and strict selectivity compared to the same reaction in solution [51] and in the gas phase [52], and minor changes in amino acid location and composition in the chromophore center may alter the potential energy surfaces, the magnitude of $S_0 \rightarrow S_1$ transition, and, eventually, its whole dynamics. bR monomerization apparently leads to certain changes in the bR_{rec} and bR_{mon} chromophore center, as seen already at the level of a shift in a maximum of their stationary absorption spectra by 9 and 15 nm, respectively. This hypsochromic shift in the stationary absorption spectra is attributed in the literature to a change in the ratio of all-*trans*/13-*cis* retinals observed during bR solubilization [21, 28]. bR containing 13-*cis* retinal, for example, 50% in DA samples of bR_{trim}, has a shorter wavelength absorption band (560 nm) and a lower extinction coefficient (55,400 $M^{-1} \cdot cm^{-1}$) [27]. However, according to data from [33] and to our data from HPLC analysis, bR_{rec} contains the same amount of all-*trans* retinal isomer (88%) as bR_{trim} (89%), while bR_{mon} contains only 71% of it (Fig. 3 and Table 1). However, the shift of the maximum during bR_{mon} solubilization is quite significant, from 568 to 553 nm, and 13-*cis* retinal level increases to 29% of total retinal content (Table 1), while during dark adaptation of bR_{trim} the maximum shifts from 568 to 560 nm, and 13-*cis* retinal level increases to approximately 60%. Therefore, the shift of the maximum of the stationary absorption spectrum and the change in photoreaction dynamics for bR_{rec} and bR_{mon} compared to bR_{trim} are apparently connected not to changes in isomeric composition of the retinal, but to some other processes the nature of which is to be clarified.

As stated above, the inner environment structure of retinal in opsin affects spectral localizations of its energy levels. The greatest effect on absorption maximum is exhibited by interaction of the protonated Schiff base of retinal with charged amino acid residues, specifically with a complex counter-ion consisting of D-212, D-85, and three water molecules [53]. This counter-ion in the monomeric form of bR is probably located closer to the protonated SB of retinal, which leads to an increase in the energy of the $S_0 \rightarrow S_1$ transition [54]. It can be proposed that inner environment structure of retinal in monomer and trimer differs. This causes a perturbation in electron levels of the retinal molecule during the transition from trimer to monomer. A perturbation in electron levels is expressed by changes in reaction dynamics for a transition from electron-excited state to primary product. In particular, the rate of this reaction slows slightly, and the quantum yield decreases slightly (the reaction becomes less effective). Unfortunately, X-ray structures of bR obtained to date in large number with satisfactory spatial resolution [11, 55] do not allow comparison of the chromophore centers of bR trimer and monomer even though many crystals pass a monomerization stage during preparation [55]. This is caused by tight molecule packing in the crystal regardless of the symmetry type, allowing the use of known X-ray structures only for bR in purple membranes.

Even though bR_{mon} and bR_{rec} molecules are located in different environments, in detergent micelles of Triton X-100 and lipid–detergent micelles of DMPC-CHAPS respectively, this most likely affects the dynamics of their primary reactions only slightly. It can be assumed that the nature of photoreactions in a monomeric form of bR is affected above all by the absence of specific natural protein–protein and protein–lipid interactions, and to a lesser degree by the composition of the artificial environment of detergents and lipid–detergent complexes.

Without having information on the structure of the chromophore center of bR in the monomeric form, what can be said about the reasons for an increase in the lifetime of bR_{mon} and bR_{rec} excited state and about the general slowing of the isomerization reaction compared to bR_{trim}? The observed rate of the photoisomerization reaction may also be affected by isomeric composition of retinals inside the bR chromophore center. The authors of a study [18] explained the two-component nature of bR_{mon} kinetic curves, describing the decay of the excited state, and an increase in the time of the fast component, compared to bR_{trim}, by the presence of higher 13-*cis* retinal content in bR_{mon} (~15%). However, it was shown [39] that the reaction of 13-*cis* retinal isomerization in the DA form of bR is barrierless in the excited state and significantly faster (~200 fs) than that of the all-*trans* retinal in the LA form (500 fs), and it strongly resembles in its characteristics the photoreaction of 11-*cis* retinal in visual pigment rhodopsin. This indicates that an increase in 13-*cis* retinal content in bR_{mon}, which was also observed in the current study, should have decreased decay time of intermediate ***I*** and not increased, as shown in the experiment. At the same time, as discussed earlier, the level of 13-*cis* retinal increases only in bR_{mon}, and kinetic parameters for the formation of primary photocycle intermediates of bR_{rec} and bR_{mon} are practically the same. This fact is most likely explained by a strong effect of protein environment on retinal, which changes during solubilization. Further studies using mutant forms of bR with substitu-

tions of amino acids in the immediate vicinity of retinal could bring us closer to understanding this effect.

Therefore, we conclude that recombinant bR obtained in the *E. coli* expression system is similar in dynamics of primary reactions to native bacteriorhodopsin in the monomeric form. All differences of bR in the monomeric form (recombinant and native) are caused by effects of the protein environment, which directs and regulates the reaction of all-*trans*→13-*cis* isomerization of retinal in bR.

Acknowledgements

The authors would like to thank the Central Scientific-Research Institute of Technology "Tekhnomash" for the kindly provided purple membranes, and V. A. Kuzmin and N. A. Durandin for assistance with registration of CD spectra of bR_{trim} and bR_{mon} samples.

This study was supported by the Russian Foundation for Basic Research (project No. 15-04-05816), Program of Fundamental Research Support of Presidium of the Russian Academy of Sciences No. 1 "Nanostructures: physics, chemistry, biology, basis of technologies", as well as National Task of Pirogov Russian National Research Medical University of the Ministry of Health of Russian Federation for 2015-2017.

REFERENCES

1. Voet, D., and Voet, J. G. (2004) in *Biochemistry* (Hoboken, N. J., ed.) 3rd Edn., Wiley & Sons, New York.
2. Henderson, R., and Shotton, D. (1980) Crystallization of purple membrane in three dimensions, *J. Mol. Biol.*, **139**, 99-109.
3. Bogomolni, R. A., Baker, R. A., Lozier, R. H., and Stoeckenius, W. (1976) Light-driven proton translocations in *Halobacterium halobium*, *Biochim. Biophys. Acta*, **440**, 68-88.
4. Hartmann, R., Sickinger, H. D., and Oesterhelt, D. (1977) Quantitative aspects of energy conversion in halobacteria, *FEBS Lett.*, **82**, 1-6.
5. Drachev, L. A., Kaulen, A. D., and Skulachev, V. P. (1984) Correlation of photochemical cycle, H^+ release and uptake, and electric events in bacteriorhodopsin, *FEBS Lett.*, **178**, 331-335.
6. Lozier, R. H., Bogomolni, R. A., and Stoeckenius, W. (1975) Bacteriorhodopsin: a light-driven proton pump in *Halobacterium halobium*, *Biophys. J.*, **15**, 955-962.
7. Danshina, S. V., Drachev, L. A., and Kaulen, A. D. (1992) The inward H^+ pathway in bacteriorhodopsin: the role of M412 and P(N)560 intermediates, *Photochem. Photobiol.*, **55**, 735-740.
8. Varo, G., and Lanyi, J. K. (1991) Thermodynamics and energy coupling in the bacteriorhodopsin photocycle, *Biochemistry*, **30**, 5016-5022.
9. Edman, K., Nollert, P., Royant, A., Belrhali, H., Pebay-Peyroula, E., Hajdu, J., Neutze, R., and Landau, E. M. (1999) High-resolution X-ray structure of an early intermediate in the bacteriorhodopsin photocycle, *Nature*, **401**, 822-826.
10. Henderson, R., Baldwin, J. M., Ceska, T. A., Zemlin, F., Beckmann, F. E., and Downing, K. H. (1990) Model for the structure of bacteriorhodopsin based on high-resolution electron cryo-microscopy, *J. Mol. Biol.*, **213**, 899-929.
11. Luecke, H., Schobert, B., Richter, H. T., Cartailler, J. P., and Lanyi, J. K. (1999) Structure of bacteriorhodopsin at 1.55 Å resolution, *J. Mol. Biol.*, **291**, 899-911.
12. Lanyi, J. K. (1999) Progress toward an explicit mechanistic model for the light-driven pump, bacteriorhodopsin, *FEBS Lett.*, **464**, 103-107.
13. Kandori, A., Kanzaki, H., Miyatake, K., Hashimoto, S., Itoh, S., Tanaka, N., Miyashita, T., and Tsukada, K. (2001) A method for detecting myocardial abnormality by using a total current-vector calculated from ST-segment deviation of a magnetocardiogram signal, *Med. Biol. Eng. Comp.*, **39**, 21-28.
14. Wang, J., and El-Sayed, M. A. (2001) Time-resolved Fourier transform infrared spectroscopy of the polarizable proton continua and the proton pump mechanism of bacteriorhodopsin, *Biophys. J.*, **80**, 961-971.
15. Sanz, C., Lazarova, T., Sepulcre, F., Gonzalez-Moreno, R., Bourdelande, J. L., Querol, E., and Padros, E. (1999) Opening the Schiff base moiety of bacteriorhodopsin by mutation of the four extracellular Glu side chains, *FEBS Lett.*, **456**, 191-195.
16. Oesterhelt, D., and Stoeckenius, W. (1974) Isolation of the cell membrane of *Halobacterium halobium* and its fractionation into red and purple membrane, *Methods Enzymol.*, **31**, 667-678.
17. Nekrasova, O. V., Wulfson, A. N., Tikhonov, R. V., Yakimov, S. A., Simonova, T. N., Tagvey, A. I., Dolgikh, D. A., Ostrovsky, M. A., and Kirpichnikov, M. P. (2010) A new hybrid protein for production of recombinant bacteriorhodopsin in *Escherichia coli*, *J. Biotech.*, **147**, 145-150.
18. Wang, J., Link, S., Heyes, C. D., and El-Sayed, M. A. (2002) Comparison of the dynamics of the primary events of bacteriorhodopsin in its trimeric and monomeric states, *Biophys. J.*, **83**, 1557-1566.
19. Dencher, N. A., and Heyn, M. P. (1982) Preparation and properties of monomeric bacteriorhodopsin, *Meth. Enzymol.*, **88**, 5-10.
20. Kovacs, I., Hollos-Nagy, K., and Varo, G. (1995) Dark adaptation and spectral changes in Triton-X-100-treated bacteriorhodopsin, *J. Photochem. Photobiol. B*, **27**, 21-25.
21. Gonzalez-Manas, J. M., Montoya, G., Rodriguez-Fernandez, C., Gurtubay, J. I. G., and Goni, F. M. (1990) The interaction of Triton X-100 with purple membrane: effect of light-dark adaptation, *Biochim. Biophys. Acta*, **1019**, 167-169.
22. Gergely, C., Zimanyi, L., and Varo, G. (1997) Bacteriorhodopsin intermediate spectra determined over a wide pH range, *J. Phys. Chem. B*, **101**, 9390-9395.
23. Pescitelli, G., and Woody, R. W. (2012) The exciton origin of the visible circular dichroism spectrum of bacteriorhodopsin, *J. Phys. Chem. B*, **116**, 6751-6763.
24. Brouillette, C. G., McMichens, R. B., Stern, L. J., and Khorana, H. G. (1989) Structure and thermal stability of monomeric bacteriorhodopsin in mixed phospholipid/detergent micelles, *Proteins*, **5**, 38-46.

25. Krebs, M. P., and Khorana, H. G. (1993) Mechanism of light-dependent proton translocation by bacteriorhodopsin, *J. Bacteriol.*, **175**, 1555-1560.
26. Tsuda, M., and Ebrey, T. G. (1980) Effect of high pressure on the absorption spectrum and isomeric composition of bacteriorhodopsin, *Biophys. J.*, **30**, 149-157.
27. Casadio, R., Gutowitz, H., Mowery, P., Taylor, M., and Stoeckenius, W. (1980) Light-dark adaptation of bacteriorhodopsin in Triton-treated purple membrane, *Biochim. Biophys. Acta*, **590**, 13-23.
28. Dencher, N. A., Kohl, K. D., and Heyn, M. P. (1983) Photochemical cycle and light-dark adaptation of monomeric and aggregated bacteriorhodopsin in various lipid environments, *Biochemistry*, **22**, 1323-1334.
29. Scherrer, P., Mathew, M. K., Sperling, W., and Stoeckenius, W. (1989) Retinal isomer ratio in dark-adapted purple membrane and bacteriorhodopsin monomers, *Biochemistry*, **28**, 829-834.
30. Song, L., Yang, D., El-Sayed, M. A., and Lanyi, J. K. (1995) Retinal isomer composition in some bacteriorhodopsin mutants under light and dark adaptation conditions, *J. Phys. Chem.*, **99**, 10052-10055.
31. Milder, S. J., Thorgeirsson, T. E., Miercke, L. J. W., Stroud, R. M., and Kliger, D. S. (1991) Effects of detergent environments on the photocycle of purified monomeric bacteriorhodopsin, *Biochemistry*, **30**, 1751-1761.
32. Braiman, M. S., Stern, L. J., Chao, B. H., and Khorana, H. G. (1987) Structure-function studies on bacteriorhodopsin. IV. Purification and renaturation of bacterio-opsin polypeptide expressed in *Escherichia coli*, *J. Biol. Chem.*, **262**, 9271-9276.
33. Greenhalgh, D. A., Farrens, D. L., Subramaniam, S., and Khorana, H. G. (1993) Hydrophobic amino acids in the retinal-binding pocket of bacteriorhodopsin, *J. Biol. Chem.*, **268**, 20305-20311.
34. Sharkov, A. V., Pakulev, A. V., Chekalin, S. V., and Matveetz, Y. A. (1985) Primary events in bacteriorhodopsin probed by subpicosecond spectroscopy, *Biochim. Biophys. Acta*, **88**, 94-102.
35. Dobler, J., Zinth, W., Kaiser, W., and Oesterhelt, D. (1988) Excited-state reaction dynamics of bacteriorhodopsin studied by femtosecond spectroscopy, *Chem. Phys. Lett.*, **144**, 215-220.
36. Gai, F., Hasson, K. C., McDonald, J. C., and Anfinrud, P. A. (1998) Chemical dynamics in proteins: the photoisomerization of retinal in bacteriorhodopsin, *Science*, **279**, 1886-1891.
37. Kobayashi, T., Saito, T., and Ohtani, H. (2001) Real-time spectroscopy of transition states in bacteriorhodopsin during retinal isomerization, *Nature*, **414**, 531-534.
38. Yabushita, A., and Kobayashi, T. (2009) Primary conformation change in bacteriorhodopsin on photoexcitation, *Biophys. J.*, **96**, 1447-1461.
39. Wand, A., Friedman, N., Sheves, M., and Ruhman, S. (2012) Ultrafast photochemistry of light-adapted and dark-adapted bacteriorhodopsin: effects of the initial retinal configuration, *J. Phys. Chem. B*, **116**, 10444-10452.
40. Govindjee, R., Balashov, S. P., and Ebrey, T. G. (1990) Quantum efficiency of the photochemical cycle of bacteriorhodopsin, *Biophys. J.*, **58**, 597-608.
41. Ye, T., Friedman, N., Gat, Y., Atkinson, G. H., Sheves, J. M., Ottolenghi, M., and Ruhman, S. (1999) On the nature of the primary light-induced events in bacteriorhodopsin: ultrafast spectroscopy of native and C13=C14 locked pigments, *J. Phys. Chem. B*, **103**, 5122-5130.
42. Briand, J., Leonard, J., and Haacke, S. (2010) Ultrafast photo-induced reaction dynamics in bacteriorhodopsin and its Trp mutants, *J. Opt.*, **12**, 1-14.
43. Mathies, R. A., Brito-Cruz, C. H., Pollard, W. T., and Shank, C. V. (1988) Direct observation of the femtosecond excited-state *cis-trans* isomerization in bacteriorhodopsin, *Science*, **240**, 777-779.
44. Song, L., El-Sayed, M. A., and Lanyi, J. K. (1993) Protein catalysis of the retinal subpicosecond photoisomerization in the primary process of bacteriorhodopsin photosynthesis, *Science*, **261**, 891-894.
45. Reyenolds, J. A., and Stoeckenius, W. (1977) Molecular weight of bacteriorhodopsin solubilized in Triton X-100, *Proc. Natl. Acad. Sci. USA*, **74**, 2803-2804.
46. Pepe, I. M., and Schwemer, J. (1987) An improved HPLC method for the separation of retinaldehyde isomers from visual pigments, *Photochem. Photobiol.*, **45**, 679-687.
47. Shelaev, I. V., Gostev, F. E., Mamedov, M. D., Sarkisov, O. M., Nadtochenko, V. A., Shuvalov, V. A., and Semenov, A. Yu. (2010) Femtosecond primary charge separation in *Synechocystis* sp. PCC 6803 photosystem I, *Biochim. Biophys. Acta*, **8**, 1410-1420.
48. Dencher, N. A., and Heyn, M. P. (1978) Formation and properties of bacteriorhodopsin monomers in the non-ionic detergents octyl-β-D-glucoside and Triton X-100, *FEBS Lett.*, **96**, 322-326.
49. Varo, G., and Lanyi, J. K. (1991) Kinetic and spectroscopic evidence for an irreversible step between deprotonation and reprotonation of the Schiff base in the bacteriorhodopsin photocycle, *Biochemistry*, **30**, 5008-5015.
50. Ahl, P. L., Stern, L. J., Düring, D., Mogi, T., Khorana, H. G., and Rothschild, K. J. (1988) Effects of amino acid substitutions in the F helix of bacteriorhodopsin. Low temperature ultraviolet/visible difference spectroscopy, *J. Biol. Chem.*, **263**, 13594-13601.
51. Hamm, P., Zurek, M., Roschinger, T., Patzelt, H., Oesterhelt, D., and Zinth, W. (1996) Femtosecond spectroscopy of the photoisomerization of the protonated Schiff base of all-*trans* retinal, *Chem. Phys. Lett.*, **263**, 613-621.
52. Coughlan, N. J. A., Catani, K. J., Adamson, B. D., Wille, U., and Bieske, E. J. (2014) Photoisomerization action spectrum of retinal protonated Schiff base in the gas phase, *J. Chem. Phys.*, **140**, 164-307.
53. Ernst, O. P., Lodowski, D. T., Elstner, M., Hegemann, P., Brown, L. S., and Kandori, H. (2014) Microbial and animal rhodopsins: structures, functions, and molecular mechanisms, *Chem. Rev.*, **114**, 126-163.
54. Hayashi, T., Matsuura, A., Sato, H., and Sakurai, M. (2012) Full-quantum chemical calculation of the absorption maximum of bacteriorhodopsin: a comprehensive analysis of the amino acid residues contributing to the opsin shift, *Biophysics*, **8**, 115-125.
55. Faham, S., and Bowie, J. U. (2002) Bicelle crystallization: a new method for crystallizing membrane proteins yields a monomeric bacteriorhodopsin structure, *J. Mol. Biol.*, **316**, 1-6.